

Theory of fast quantum control of exciton dynamics in semiconductor quantum dots

C. Piermarocchi, Pochung Chen, Y. S. Dale, and L. J. Sham

Department of Physics, University of California San Diego, La Jolla, California 92093-0319

(Received 13 September 2001; published 18 January 2002)

Optical techniques for the quantum control of the dynamics of multiexciton states in a semiconductor quantum dot are explored in theory. Composite bichromatic phase-locked pulses are shown to reduce the time of elementary quantum operations on excitons and biexcitons by an order of magnitude or more. Analytic and numerical methods of designing the pulse sequences are investigated. Fidelity of the operation is used to gauge its quality. A modified quantum Fourier transform algorithm is constructed with only Rabi rotations and is shown to reduce the number of operations. Application of the designed pulses to the algorithm is tested by a numerical simulation.

DOI: 10.1103/PhysRevB.65.075307

PACS number(s): 78.67.Hc, 03.67.Lx

I. INTRODUCTION

The possibility of controlling the dynamics of a quantum system has long captured the attention of workers in a wide range of physical systems. Quantum control can be realized by engineering a time-dependent Hamiltonian that depends on a finite set of parameters. In quantum chemistry, this engineering has led to the possibility of driving chemical reactions using tailored laser pulses and external fields.¹ Quantum control has been recently extended to semiconductor nanostructures leading, for instance, to controlled currents,² coherent control of excitons^{3,4} and electron spin,⁵ and controlled intersubband transitions of shallow donors using terahertz radiation.⁶

In this paper we explore optical control of the ultimate quantum device in semiconductor nanotechnology, i.e., a quantum dot. In a semiconductor quantum dot the electronic levels have a density of states characteristic of a single atom. Yet, the dot is a *mesoscopic* system, i.e., in contrast to the single-atom case, the quantization of the electronic levels is realized within a system that contains actually 10^5 – 10^6 atoms. A key ingredient in the quantum control of these semiconductor nanostructures is the robustness of the elementary excitation, the exciton. An electron-hole pair optically excited in an undoped quantum dot feels the presence of the large number of atoms in the material only through the static dielectric constant and the electron and hole effective mass.⁷ This allows us to treat excitons as excitations in giant atoms and to control excitons with optical techniques similar to those used for the manipulation of atoms and molecules. However, unlike the atomic case, the dot is in a solid-state environment with the attendant decoherence. We shall also make use of the conduction-band electron and the valence-band hole as the constituents of an exciton. A quantum dot is like an empty box that can be filled with multiexciton complexes composed of many interacting excitons.⁸ In these multiexciton states, the Coulomb correlation is taken into account and yet the spin configuration is transparent. The spin configuration can then be controlled by the light polarization of the optical pulses.

The implementation of quantum algorithms is a particular case of quantum control. The potentialities of semiconductor

quantum dots in the implementation of quantum algorithms have been readily recognized,^{9–11} as well as in conjunction with optical microcavities.^{12–14} The use of optical control of excitons in dots for quantum operations has been suggested,¹⁵ and a theory for the physical implementation of quantum algorithms in a dot using ultrafast optical pulses was investigated.¹⁶ Ideas for a scalable quantum computer involving excitons in different dots and optical quantum control were proposed.^{12,17,18} Advances in ultrafast optics in quantum dots make possible the manipulation of electronic excitations in a semiconductor nanostructure with time resolution in the femtosecond domain. So far, frequency selection is used to avoid unwanted transitions to states out of the computational space. Laser pulses of a narrow frequency range are too long in duration compared with the decoherence time for quantum operations. Thus, a design of fast control is necessary. A fast control allows us to make a reasonable number of operations well within the decoherence time. It may also be made an ingredient in the realization of sophisticated error correction and decoupling schemes.¹⁹ We will give an explicit design for the realization of fast control of two qubits encoded in two antiparallel-spin excitons in a single quantum dot. The slight increase in complexity of the optical setup is within the capability of the current experiments. An optimal design is an inverse problem to the finding a state given the Hamiltonian: the issue is to find a time-dependent optical electric field that produces a desired result in the shortest time as possible. The required experimental resources are realistic: lasers generating Gaussian pulses with two different frequencies that can be phase locked. The synthesis of phase-locked optical pulse from separate femtosecond lasers has been recently reported,²⁰ and here we propose an important application of this technique. We explore the three different approaches to the control problem: an intuitive one making use of the area theorem²¹ and also give an analytical tool, the cluster expansion of the evolution operation, much used in nuclear magnetic resonance (NMR) spectroscopy,²² and numerical optimization.

The implementation of a two-qubit quantum Fourier transform²³ (QFT) is used as a test case for the different methods of design. Any algorithm can be decomposed as

series of single-qubit rotations and two-qubit conditional rotations.²³ A series of two-color phase-locked optical pulses is suggested to realize the fast control of these fundamental rotations. Fidelity²⁴ is used to gauge the quality of the operations and of the complete algorithm of QFT within the decoherence time. Error correction could be added later to improve the result.

The paper is organized as follows. Section II gives the structure of the multiexciton states from a microscopic model for a quantum dot. Section III explains the principles of three methods of design of optical pulses for a fast control in a subspace of multiexciton states and compares their results in fundamental quantum operations. Section IV contains a numerical simulation of the QFT algorithm in a quantum dot. The simulation takes into account the microscopic details of the laser-exciton dynamics, including decoherence and the presence of multiexciton levels outside the computational space. Details of the decomposition of the QFT in terms of only Rabi rotations for a general n -qubit system are relegated to the appendix. Section V summarizes and draws a number of conclusions. A brief description of the key idea of pulse shaping and the application to a different quantum algorithm were published in Ref. 16.

II. MULTIEXCITON STATES

The energies and wave functions of the multiexciton states in a dot are calculated starting from two confined levels of electrons and holes each in a parallelepiped QD.²⁵ The electronic levels included are the first two states deriving from the localization of s -like conduction-band states. They carry a spin $\pm \frac{1}{2}$. The hole levels derive from the localization of states in the p -like valence-band heavy holes carrying a $\pm \frac{3}{2}$ total spin in the direction of the growth axis. The size of the dot, $40 \times 35 \times 5 \text{ nm}^3$, is typical of interface fluctuation quantum dots.²⁶ Only Coulomb interaction between the carriers, which conserves their conduction- or valence-band indices is taken into account exactly. This amounts to neglecting the electron-hole exchange, which gives a fine structure of the excitonic levels depending on the symmetry of the dot. We calculated this effect to be of the order of a few $\mu \text{ eV}$, which can thus be safely neglected in the discussion of fast control considered in this paper. Figure 1 shows the energy structure of the multiexciton states. The multiexciton levels include zero, one, two, three, and four excitons in the dot. The choice of two levels each of electrons and holes limits the resultant number of excitons to four. The $+$ or $-$ refers to the polarization of the light that has to be used to create each exciton. Only optically active multiexciton states are shown. Since the optically forbidden multiexciton states are not the source of unintended dynamics, they are removed from the following discussion. Our model adopts the measured dipole moment of 75 D for the single exciton in a single GaAs fluctuation dot²⁷ and the transition-matrix elements between the multiexciton states are then calculated. The later values are used in the numerical simulations in Sec. IV. Note that the values of the dipole moments in this kind of systems are one or two orders of magnitude higher than those of atoms. Theoretical estimates suggest that this giant

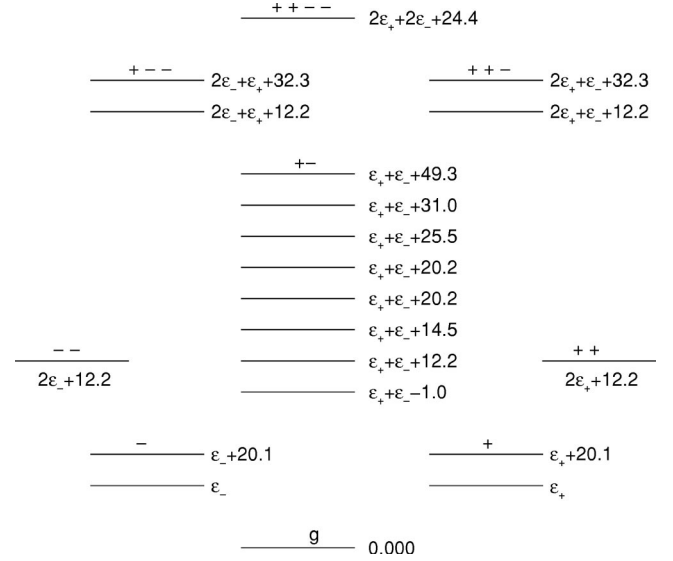


FIG. 1. Energy levels of the multiexciton states in a quantum dot in meV. $\epsilon_+ = \epsilon_- = 1764 \text{ meV}$.

dipole effect seems to be stronger in quantum dots generated by monolayer fluctuations than the self-assembled dots.²⁸

III. QUANTUM CONTROL OF MULTIEXCITON STATES

A. Formulation of the problem

Quantum control consists in the design of a time-dependent addition to the system Hamiltonian, which will drive the state of the system from a prepared state to a designated state within a number of desirable conditions. In this paper, we shall focus on the dynamics of two excitons in a quantum dot. The controlling agent is a sequence of laser pulses. The dynamics of this two-exciton system not only serves as a powerful illustration of the more general case of multiple discrete states but also to form a set of “universal gates,” i.e., fundamental operations in terms of which any quantum computation may be constructed.²³ The system is not closed. In addition to the laser interaction, the quantum dot has other excitonic states and its environment of the substrate and other dots is a source of decoherence. The time limitation due to decoherence and the resonance conditions to avoid the unintended dynamics form two contradictory requirements under which the dynamics of the two excitons in a dot must be optimized.

For the system of two excitons, we use a basis set of four states in the following orders the ground state $|0\rangle$, the two excitons with the lowest energy at 1764 meV above the ground state and opposite polarizations denoted by $|+\rangle$ and $|-\rangle$, and the biexciton state $|-\rangle|+\rangle$ at 3527 meV. A $\sigma+$ polarized photon can drive the excitonic transition $|0\rangle \rightarrow |+\rangle$ and the biexcitonic transition $|-\rangle \rightarrow |-\rangle|+\rangle$. The two transitions have different energies due to the Coulomb binding energy of the biexciton. We can write the Hamiltonian of the four-level systems coupled to an external electromagnetic field with σ^+ polarization, treated classically, in the form

$$H^+ = \begin{bmatrix} 0 & \Omega_+(t)/2 & 0 & 0 \\ \Omega_+^*(t)/2 & \epsilon_+ & 0 & 0 \\ 0 & 0 & \epsilon_- & f\Omega_+(t)/2 \\ 0 & 0 & f\Omega_+^*(t)/2 & \epsilon_{-+} \end{bmatrix}, \quad (1)$$

where $\Omega_+(t) = \sum_j d_+ E_{+,j}(t - \tau_j)$ represents a time-dependent Rabi energy provided by a train of phase-locked optical pulses. The dipole moment of the exciton $|+\rangle$ is denoted by d_+ and f is a correction factor to the dipole moment in the exciton-biexciton transition-matrix element due to Coulomb interaction. The amplitude of the electric field $E_{+,j}(t - \tau_j) = \mathcal{E}_{+,j}(t - \tau_j) e^{-i\omega_+(t - \tau_j)} e^{i\phi_j}$ is assumed to be slowly varying. As in the atomic case, the condition $\omega_+ \gg d_+ \mathcal{E}_{+,j}$ enables the rotating-wave approximation to be used in H^+ above. Thus, the counter-rotating terms, such as $H_{0,-}^+ = \Omega_+^*/2$, are set to zero. Similarly the Hamiltonian associated with a σ_- polarized electric field is given by

$$H^- = \begin{bmatrix} 0 & 0 & \Omega_-(t)/2 & 0 \\ 0 & \epsilon_+ & 0 & f\Omega_-(t)/2 \\ \Omega_-^*(t)/2 & 0 & \epsilon_- & 0 \\ 0 & f\Omega_-^*(t)/2 & 0 & \epsilon_{-+} \end{bmatrix}. \quad (2)$$

For simplicity of exposition we consider a sequence of nonoverlapping pulses, although in numerical simulations we have found it possible to pack the pulses with 10% overlap with negligible deterioration. Thus, we write the unitary time-evolution operator from $t = \tau_0$ to $t = T$ in the form

$$U(T, \tau_0) = \prod_{j=1}^N U_j^{\sigma_j}(\tau_j, \tau_{j-1}), \quad (3)$$

where N indicates the number of pulses in the train and τ_j, τ_{j-1} denote the beginning and the end of the j th pulse. For a given quantum operation $U(T, \tau_0)$, the time optimization can be viewed as consisting of two components. The first is to have a minimum number of pulses N in Eq. (3). Optical pulses can directly perform Rabi rotations with generators σ_x and σ_y but rotations with generator σ_x need to be built as a combination of σ_y and σ_z . In our design of the laser implementation of a quantum algorithm we try to decompose the required global transformation directly in rotations generated by σ_y and σ_x for both single-qubit and conditional operations without appealing to Hadamard, controlled-NOT, or conditional phase shift. We have demonstrated this by the construction of the Deutsch-Josza algorithm¹⁶ and the quantum Fourier transform (see below). Since the saving is not exponential, in theory it may be considered trivial, but in practice, especially in the initial stage of experimental implementation, the use of the right decomposition of the algorithms may be advantageous.

The second component for a fast control is the time optimization of each pulse in the product of Eq. (3), which is the main subject of this section. Consider the case of a σ_+ pulse. In the interaction representation, $\tilde{O} = \Lambda O \Lambda^\dagger$ denotes the transformed operator from O , with $\Lambda(t) = e^{iH_0 t}$, where H_0 is a diagonal matrix with elements $(0, \epsilon_+, \epsilon_-, \epsilon_{-+})$. The term $U_j^{\sigma_j}$ in Eq. (3) becomes for σ_+ pulse (with j understood below)

$$\tilde{U}^{\sigma_+} = T \exp \left[-i \frac{1}{2} \int_0^\tau dt \tilde{V}^{\sigma_+}(t) \right], \quad (4)$$

where $\tilde{V}(t)^{\sigma_+}$ is

$$\begin{bmatrix} 0 & \Omega_+(t) e^{i\epsilon_+ t} & 0 & 0 \\ \Omega_+^*(t) e^{-i\epsilon_+ t} & 0 & 0 & 0 \\ 0 & 0 & 0 & f\Omega_+(t) e^{i(\epsilon_+ - \Delta)t} \\ 0 & 0 & f\Omega_+^*(t) e^{-i(\epsilon_+ - \Delta)t} & 0 \end{bmatrix} \quad (5)$$

and $\Delta = \epsilon_+ + \epsilon_- - \epsilon_{-+}$ is the biexciton binding energy. When only a circularly polarized light is used, Eq. (5) shows that the four-level system behaves as a double two-level system, the first-two-level transition (exciton transition) being represented by $|0\rangle \rightarrow |+\rangle$ and the second (biexciton transition) by $|-\rangle \rightarrow |-\rangle$.

Consider now the desired operation where the exciton transition is a Rabi rotation through angle α and the biexciton transition is a Rabi rotation through α' ,

$$\tilde{U}_j^{\sigma_+} = \begin{bmatrix} \cos(\alpha/2) & -\sin(\alpha/2) & 0 & 0 \\ \sin(\alpha/2) & \cos(\alpha/2) & 0 & 0 \\ 0 & 0 & \cos(\alpha'/2) & -\sin(\alpha'/2) \\ 0 & 0 & \sin(\alpha'/2) & \cos(\alpha'/2) \end{bmatrix}. \quad (6)$$

The most direct solution for the realization of this transformation would be a two-pulse combination,

$$E_+(t) = \mathcal{E}_0 e^{-(t/\epsilon)^2} e^{-i\omega_0 t} + \mathcal{E}_1 e^{-(t/\epsilon_1)^2} e^{-i\omega_1 t + i\phi}. \quad (7)$$

If the two pulses are resonant, respectively, with the two transitions, i.e., $\omega_{0+} = \epsilon_+$ and $\omega_{1+} = \epsilon_{-+} - \epsilon_-$, and sufficiently narrow in frequency, the pulse resonant with the exciton transition would have negligible effect on the biexciton transition and vice versa. However, this has been shown to be costly in time.¹⁶ The problem is to find a composite pulse that would take much less time with tolerable deterioration of quality of the transformation.

For the quality of the transformation, we follow Ref. 24 in defining the fidelity of the transformation as

$$F = \overline{|\langle \psi_{\text{in}} | \tilde{U}^\dagger U_i | \psi_{\text{in}} \rangle|^2}, \quad (8)$$

where U_i is the ideal unitary operation \tilde{U} is the unitary transformation generated by the optical pulses, and the overline denotes the average over all the possible initial states. The operator $\tilde{U}^\dagger U_i$ is denoted by I for short. The average over all the possible states is done by considering an initial state with arbitrary complex coefficients $|\psi_{\text{in}}\rangle = \sum_j c_j |j\rangle$ with the normalization constraint $\sum_j |c_j|^2 = 1$. The fidelity can be then written in the form

$$F = \sum_{ijkl} \overline{c_i^* c_j c_k^* c_l I_{ij} I_{lk}^*} \quad (9)$$

and, in the four-level system considered here, the overline average is then on a hypersphere S in C^8 determined by the normalization condition. This average $(1/S) \int_S d^2 c_1 d^2 c_2 d^2 c_3 d^2 c_4 c_i^* c_j c_k^* c_l$ is easily evaluated in polar coordinates and gives

$$F = \frac{1}{10} \sum_i |I_{ii}|^2 + \frac{1}{20} \sum_{i \neq j} (I_{ii} I_{jj}^* + I_{ij}^* I_{ij}). \quad (10)$$

The difference of the coefficients from those of Ref. 24 is due to their additional restrictions on the coefficients c_j . Our choice gives a more conservative estimation of the error in the operations.

B. Pulse design

In this section, we explain three different approaches to pulse design to shorten the time of the quantum operation.

1. Approximation by the area theorem

In the limit of very long pulses, the area theorem²¹ determines the intensity of a Gaussian pulse that has to be used for a given rotation α ,

$$\mathcal{E}_0 = \frac{\alpha}{s \sqrt{\pi d_+}}. \quad (11)$$

For a single two-level system the pulse width s in Eq. (11) can be made arbitrarily small, but in the four-level case we are strongly limited by the resonance condition to $1/s$,

$\mathcal{E}_0 d_+ \ll \Delta$. In order to shorten the time duration of the whole pulse, an intuitive approach would be to allow the two components of Eq. (7) to overlap in frequency but keep each satisfying the area theorem.

2. The average Hamiltonian method

The cumulant expansion (also known as the Magnus expansion²⁹) of the evolution operator $\tilde{U}_j^{\sigma+}$ in Eq. (4) is given by²²

$$\tilde{U}_j^{\sigma+} = \exp \left[-\frac{1}{2} (\tilde{V}_1 + \tilde{V}_2 + \dots) \right]. \quad (12)$$

The first term of the expansion corresponds to a time average of the interaction Hamiltonian,

$$\tilde{V}_1 = \int_0^\infty dt \tilde{V}(t). \quad (13)$$

The second term is given by

$$\tilde{V}_2 = \frac{-i}{4} \int_0^\infty dt \int_0^t dt' [\tilde{V}(t), \tilde{V}(t')]. \quad (14)$$

Keeping only the first term in the exponent constitutes the average Hamiltonian approximation. An estimation of the error in the truncation of the cumulant expansion is given by the second term.

3. Numerical approach

The parameters in Eq. (7) are varied to find the maximum fidelity. To lessen the numerical effort, physical considerations guide the reduction of the number of parameters varied. The first two approximation methods are also useful as starting points.

C. Examples of pulse design

We illustrate the above methods for a single-qubit operation, i.e., a parallel rotation of both the exciton and biexciton transitions. For simplicity, let $f=1$ and $s_1=s$. Both theoretical estimates and experimental measurements have an f value not far from unity. In any case, the extension to $f \neq 1$ can be made in a manner similar to the treatment of the conditional rotation given below. We consider a composite pulse by superposing and phase locking the two pulses in Eq. (7) with $\mathcal{E}_0 = \mathcal{E}_1$, $\omega_{0+} = \epsilon_+$, and $\omega_{1+} = \epsilon_+ - \Delta$. It remains to choose a value for $\mathcal{E}_0(s)$ by each of the three methods above and tests its efficacy by evaluating the fidelity of the operation.

In Fig. 2(a) the fidelity for $\alpha = \alpha' = \pi$ rotation is plotted as a function of the temporal width of the Gaussian pulse s . The corresponding value for the peak of the Rabi energy $\Omega_0 = d_+ \mathcal{E}_0(s)$ is also given in Fig. 2(b). The value of the biexcitonic binding energy Δ is 1 meV. The results of the area-theorem approximation are shown as the dashed lines. The fidelity is close to unity only for $s \gg 1/\Delta$, corresponding to a region where the frequency selectivity is preserved. If, for instance, a 98% fidelity is required, the area-theorem ap-

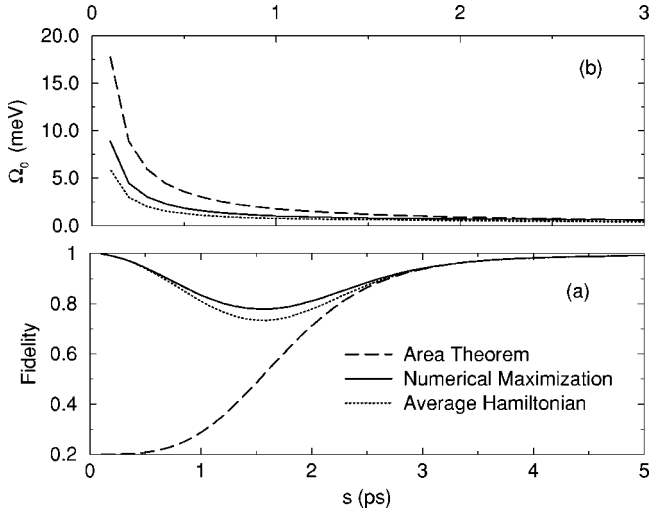


FIG. 2. (a) Fidelity as a function of the temporal width of the Gaussians s for a parallel rotation of $\alpha = \alpha' = \pi$. (b) Peak value of the Rabi energy $\Omega_0 = d_+ \mathcal{E}_0(s)$. Dashed lines: the area-theorem approximation. Dotted lines: the average Hamiltonian approximation. Solid lines: numerical maximization of the fidelity.

proach will lead to optical pulses with $s > 4$ ps. The area theorem is not the best procedure of time optimization for single-qubit operations.

Applying the average Hamiltonian approximation to the restricted pulse specified above leads to the single-qubit rotation $\tilde{U}^{\sigma+}$ in the form of Eq. (6) with chosen values for $\alpha = \alpha'$ and for s , leading to \mathcal{E}_0 given by

$$\mathcal{E}_0 = \frac{\alpha}{s \sqrt{\pi} d_+ (1 + e^{-(\Delta s/2)^2})}. \quad (15)$$

The Gaussian term in the denominator on the right gives a correction to the area theorem, Eq. (11). The results are shown as dotted lines in Fig. 2(b). An estimate of the error of the average Hamiltonian approximation may be made by evaluating the second-order term in the cluster expansion given by Eq. (14). A rough estimate is provided by replacing the Gaussians with square pulses of width s ,

$$\tilde{V}_2 = (d_+ \mathcal{E}_0 \Delta)^2 [\sin(\Delta s) - \Delta s + 2 \Delta s \cos(\Delta s/2) - 4 \sin(\Delta s/2)] \Xi = \phi \Xi, \quad (16)$$

where Ξ is a diagonal matrix with elements $(-\frac{1}{2}, \frac{1}{2}, \frac{1}{2}, -\frac{1}{2})$. Expanding in the limit of short pulses $\Delta s \ll 1$ we get $\phi \sim -(d_+ \mathcal{E}_0 / \Delta)^2 (\Delta s)^3 / 3$. The correction to the area theorem in the first-order term, Eq. (15), is by contrast $\sim (d_+ \mathcal{E}_0 / \Delta) (\Delta s)$. Faster pulses make the lowest order $\tilde{V}_1 \gg \tilde{V}_2$. The resultant fidelity by the average Hamiltonian method is shown as dotted lines in Fig. 2(a). Note that it is possible to obtain a 98% fidelity using much shorter pulses, of the order of 100 fs. In the limit of very short pulses this correspond to pulses spectrally very broad, which do not distinguish between the two transitions but yield a nearly parallel rotation.

The results of the numerical maximization using one variable \mathcal{E}_0 by Brent's method³⁰ are plotted as solid lines. The

optimal curve $\mathcal{E}_0(s)$ deviates considerably at short times from the area-theorem approximation but is close to the average Hamiltonian approximation throughout the whole range of s .

The second example is a conditional operation for two qubits, viz. a σ_+ biexcitonic transition without affecting the excitonic $|+\rangle \rightarrow |0\rangle$, i.e., a rotation \tilde{U}_j in Eq. (6) with $\alpha = 0$ and $\alpha' = \pi$. For the combined pulse in Eq. (7) we consider now $\phi = \pi$, and again $\mathcal{E}_0 = \mathcal{E}_1$ and $\omega_{0+} = \epsilon_+$, $\omega_{1+} = \epsilon_+ - \Delta$.

From the average Hamiltonian approximation (the first-order term in the cluster expansion), we obtain relations for the three parameters of the pulse \mathcal{E}_0 , s , and s_1 for the desired rotations,

$$\alpha = d_+ \mathcal{E}_0 \sqrt{\pi} (s - s_1 e^{-(\Delta s_1/2)^2}), \quad (17)$$

$$\alpha' = d_+ \mathcal{E}_0 \sqrt{\pi} (s_1 - s e^{-(\Delta s/2)^2}). \quad (18)$$

For a given value of s_1 , the other two parameters may be solved in the case with $\alpha = 0$ and $\alpha' = \pi$,

$$s = s_1 e^{-(\Delta s_1/2)^2}, \quad (19)$$

$$\mathcal{E}_0 = \sqrt{\pi} / d_+ (s_1 - s e^{-(\Delta s/2)^2}). \quad (20)$$

In the limit of large Δ the solution gives $s \rightarrow 0$ eliminating the term resonant with the excitonic transition and $\mathcal{E}_0 \rightarrow \sqrt{\pi} / s_1 d_+$ in accord with the area theorem for the biexcitonic transition. For $\Delta \neq 0$ this system has always a solution for any $\alpha \neq \alpha'$. Correction to the average Hamiltonian approximation may be estimated in analogy with the parallel rotation case in the limit $s_1, s \ll 1/\Delta$ and give for \tilde{V}_2 a diagonal matrix with elements $(-\phi_1/2, \phi_1/2, -\phi_2/2, \phi_2/2)$, where

$$\phi_1 \sim \frac{1}{32} \left(\frac{d_+ \mathcal{E}_0}{\Delta} \right)^2 [(\Delta s)^3 + 2(\Delta s_1)^3 - 3(\Delta s)(\Delta s_1)^2],$$

$$\phi_2 \sim \frac{1}{96} \left(\frac{d_+ \mathcal{E}_0}{\Delta} \right)^2 [(\Delta s_1)^3 + 2(\Delta s)^3 - 3(\Delta s_1)(\Delta s)^2].$$

In Fig. 3 we show (a) the fidelity and (b) the peak Rabi energy for the $\alpha = 0$ and $\alpha' = \pi$ transformation for all three methods. The area-theorem approximation amounts to taking a single pulse resonant with the biexciton transition. For the numerical maximization we maximize the fidelity for a given s_1 value as a function of s and \mathcal{E}_0 using the downhill simplex method.³⁰ We see clearly that the average Hamiltonian again gives a very good approximation: the deviations from the numerical maximization are negligible in most of the region. Also in this case we see that the use of a composite pulse provide a considerable saving in the time for the operation.

As a last example, we investigate whether a single square pulse shape can serve the function of the two overlapping pulses. For a square pulse, an exact analytical expression for \tilde{U}^+ can be given. It has been suggested³¹ that off-resonant unwanted transitions can be corrected using square pulses.

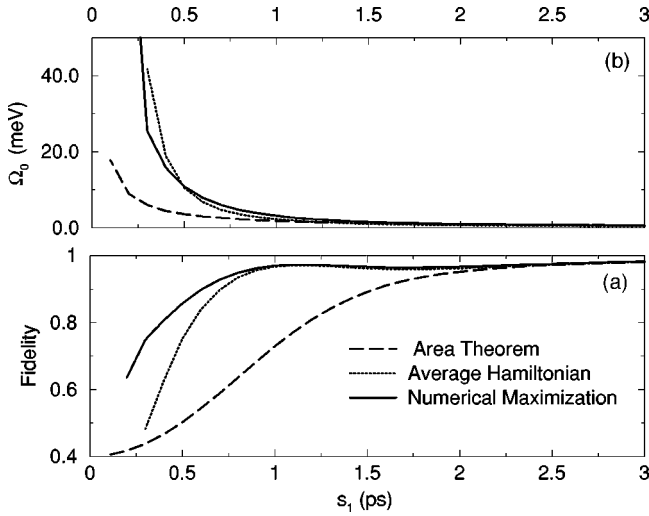


FIG. 3. (a) Fidelity as a function of the temporal width s_1 of the biexciton Gaussian component in the composite pulse for a rotation of $\alpha' = \pi$ only for the biexciton transition. (b) Peak value of the Rabi energy. Dashed lines: the area-theorem approximation with a single pulse resonant with the biexciton transition. Dotted lines: the averaged Hamiltonian approximation. Solid lines: numerical maximization of the fidelity.

The specific case discussed above this corresponds to the use of a single pulse resonant with the biexciton transition with s_1 satisfying the conditions

$$s_1 \Delta = \sqrt{4m^2 - 1} \pi \hbar, \quad (21)$$

$$s_1 \Omega_+ = \pi, \quad (22)$$

with integer m . Equation (22) gives a π rotation for the biexcitonic transition in accord with the area theorem, and the condition in Eq. (21) sets to zero the off-diagonal terms in the 2×2 block corresponding to the excitonic transition. However, additional phases in the diagonal corresponding to a σ_z rotation for the exciton transitions are introduced, which decrease the fidelity of the operation. We calculate the fidelity and peak Rabi energy for a conditional π rotation using a single square pulse resonant with the biexcitonic transition as functions of the temporal width s_1 of the square pulse and compare it with the shaped pulse result of the average Hamiltonian approximation in Fig. 4. In the comparison, note that s_1 in the square wave is the temporal width but in the shaped pulse is the half-width of the biexciton Gaussian component. The fidelity of the square wave shows oscillations with maxima roughly corresponding to the conditions in Eqs. (21) and (22) but never reaches as high as the two-pulse case. Moreover, the spread in frequency of the square-pulse spectrum is a source for unintended dynamics for higher exciton energy levels in the physical dot, while Gaussian pulses avoid this problem.

IV. QUANTUM FOURIER TRANSFORM

The theory of control of the two excitons will now be applied to construct a physical implementation of a quantum algorithm, the two-qubit quantum Fourier transform. One qu-

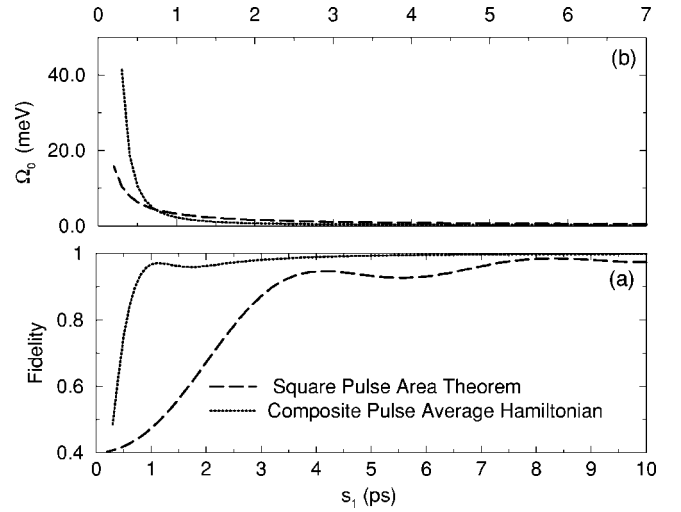


FIG. 4. (a) Fidelity as a function of the temporal width s_1 of the square pulse and of the biexciton Gaussian component of the shaped pulse, for a rotation of $\alpha' = \pi$ only for the biexciton transition. (b) Peak value of the Rabi energy. Dashed lines: when a single square pulse resonant with the biexciton transition and the area theorem is used. Dotted lines: composite Gaussian pulse using the average Hamiltonian approach, same as the dotted lines in Fig. 3.

bit is given by the presence or absence of a σ^+ polarized exciton in the dot and the second qubit by the σ^- exciton. For the single-qubit operation we have to act both in the exciton and in the biexciton transition. The case of parallel π rotation discussed in the preceding section corresponds, therefore, to a single-qubit operation on the first qubit. As a conditional two-qubit gate we use a controlled-ROT operation, which is essentially the controlled-NOT operation with a π rotation replacing the logical NOT operation. The controlled-ROT is the conditional dynamics of adding to the quantum dot a σ_+ exciton only if an exciton with σ_- polarization is already there. This corresponds to a σ_+ biexcitonic transition⁹ without affecting the excitonic $|+\rangle \rightarrow |0\rangle$. The second example discussed in the preceding section is a CROT controlled by second qubit, i.e., by the σ_- exciton. Single-qubit and conditional rotations are easily generalized to arbitrary angles. The exact mapping for the four-level system to two qubits is given by

$$\{|0\rangle, |+\rangle, |-\rangle, |-\rangle\} \rightarrow \{|00\rangle, |01\rangle, |10\rangle, |11\rangle\}. \quad (23)$$

Unlike the NMR implementations, it is not possible here to make use of the free evolution of the interacting qubits since it requires keeping track of the oscillation at the optical frequency and, therefore, an optical control over several picoseconds with subfemtosecond accuracy. By working in the interaction representation, we get rid of this drift term, making the design of the control more convenient. At the end of the sequence of pulses for a given algorithm the interaction representation does not affect the computation since the read-out is always done in an eigenstate of the system. Therefore the control of the qubit is always active and is constructed in terms of rotations with σ_x and σ_y generators between pairs of levels in the four-level system.

The QFT is the key ingredient in a number of important quantum algorithms, in particular, Shor's factorization.²³ Consider an n -qubit state

$$|x\rangle \equiv |x_n \cdots x_1\rangle, \quad \text{where } x = \sum_{i=1}^n x_i 2^{i-1}. \quad (24)$$

The QFT is defined as a linear operator on an orthonormal basis of $|0\rangle, \dots, |N-1\rangle$, where $N=2^n$, with the action

$$U_{\text{QFT}}|x\rangle = \frac{1}{\sqrt{N}} \sum_{q=0}^{N-1} e^{2\pi i x q/N} |q\rangle \quad (25)$$

analogous to the construction of Bloch states in a one-dimensional chain. The standard way to construct QFT employs two basic operations: the Hadamard gate on the j th qubit H_j and the conditional phase gate S_{jk} , where j is the control qubit and k is the target qubit.²³ The two-qubit QFT can be realized, for instance, by the simple sequence $H_2 S_{2,1} H_1$. However, if we decompose each of the three operations in Rabi rotations we end up using more optical pulses than necessary. In fact, each Hadamard transformation requires at least two optical pulses $R_j(\pi, \hat{x}) R_j(\pi/2, \hat{y})$, where $R_j(\theta, \hat{\epsilon})$ is the rotation of the j th qubit in the $\hat{\epsilon}$ direction with angle θ . Following the decomposition in Ref. 32, we find S_{12} with the sequence

$$\begin{aligned} & R_1\left(-\frac{\pi}{2}, \hat{y}\right) C_{2,1}^{\text{ROT}}\left(\frac{\pi}{2}, \hat{x}\right) C_{2,1}^{\text{ROT}}\left(-\frac{\pi}{2}, \hat{x}\right) R_1\left(\frac{\pi}{2}, \hat{x}\right) \\ & R_1\left(\frac{\pi}{2}, \hat{y}\right) R_2\left(-\frac{\pi}{2}, \hat{y}\right) R_2\left(\frac{\pi}{2}, \hat{x}\right) R_2\left(\frac{\pi}{2}, \hat{y}\right). \end{aligned} \quad (26)$$

In $C_{j,k}^{\text{ROT}}$, j is the control qubit and k is the target. For example,

$$C_{2,1}^{\text{ROT}}(\theta, \hat{x}) = \begin{bmatrix} 1 & 0 & 0 & 0 \\ 0 & 1 & 0 & 0 \\ 0 & 0 & \cos(\theta/2) & -i \sin(\theta/2) \\ 0 & 0 & -i \sin(\theta/2) & \cos(\theta/2) \end{bmatrix}, \quad (27)$$

and the bar over subscript 2 indicates a rotation of the target only for the control qubit in the state 0,

$$C_{2,1}^{\text{ROT}}(\theta, \hat{x}) = \begin{bmatrix} \cos(\theta/2) & -i \sin(\theta/2) & 0 & 0 \\ -i \sin(\theta/2) & \cos(\theta/2) & 0 & 0 \\ 0 & 0 & 1 & 0 \\ 0 & 0 & 0 & 1 \end{bmatrix}. \quad (28)$$

The total number of pulses for the QFT is then 12.

We redefine the QFT as

$$U_{\text{MQFT}} = B U_{\text{QFT}} \Sigma, \quad (29)$$

where Σ is the all-qubit inversion ($x_i \rightarrow 1 - x_i$),

$$\Sigma|x\rangle = |\bar{x}\rangle, \quad \text{where } \bar{x} = \sum_{i=1}^n (1 - x_i) 2^{i-1}, \quad (30)$$

and B is the transformation ($x_i \rightarrow x_{n-i+1}$), which may be termed boustrophedon,³³

$$B|x_n \cdots x_2 x_1\rangle = |x_1 x_2 \cdots x_n\rangle = |\bar{x}\rangle. \quad (31)$$

In the Appendix, we prove that U_{MQFT} is a composition of rotations of generators σ_x and σ_y for states of any number of qubits, denoted by U_{MQFT} . By avoiding the pulse-consuming S_{ij} , this saves time by using a smaller number of pulses than U_{QFT} . U_{MQFT} can be used directly in phase estimation or factorization algorithms without the need for B and Σ , the global qubit transformations, which are just relabeling of the qubits. In a physical implementation there is the possibility to make global qubit transformations that are simple relabeling, at no cost from the point of view of the quantum control. If, for instance, a quantum computer is composed of a chain of $\frac{1}{2}$ spins, at any time we can decide to flip all spin up into spin down and vice versa. This all-bit inversion is a simple relabeling. We do not need to apply any pulse to the chain; we have just to remember that in the readout. The same can be done by switching in reading the string of qubits from the right to the left instead of from left to right, which corresponds to the boustrophedon transformation in Eq. (31). Although this saving in time is of the order polynomial in n , for the current attempt at physical implementation of prototype quantum computers it could provide a helpful simplification of the experimental procedure.

For $n=2$, $N=4$ the pulse sequence for U_{MQFT} is

$$C_{2,1}^{\text{ROT}}\left(\frac{\pi}{2}, \hat{x}\right) R_2\left(-\frac{\pi}{2}, \hat{y}\right) R_2\left(\frac{\pi}{4}, \hat{x}\right) R_1\left(-\frac{\pi}{2}, \hat{y}\right). \quad (32)$$

We carried out a numerical simulation of the dynamics of the multiexciton levels for this MQFT algorithm with and without the use of composite pulses. We took the peak of the Rabi energy to be 2 meV, larger than the 1 meV binding energy of the biexciton. The width of the pulses is calculated using the area-theorem approximation and the average Hamiltonian. The corresponding values of fidelity for U_{MQFT} are 0.257 and 0.992. The pulse sequence is completed within 6 ps.

In order to check the robustness of the use of composite pulses in the presence of dephasing, we include the spontaneous emission in the simulation by adding the Lindblad operators in the equation of motion for the density matrix³⁴

$$\frac{d}{dt} \rho = -\frac{i}{\hbar} [H, \rho] + \sum_{j=1}^4 (L_j \rho L_j^\dagger - \frac{1}{2} \rho L_j^\dagger L_j - \frac{1}{2} L_j^\dagger L_j \rho), \quad (33)$$

where

$$\begin{aligned} L_1 &= \sqrt{\Gamma} |0\rangle\langle +|, & L_2 &= \sqrt{\Gamma} |0\rangle\langle -|, \\ L_3 &= \sqrt{\Gamma} |+ \rangle\langle - +|, & L_4 &= \sqrt{\Gamma} |- \rangle\langle - +|, \end{aligned} \quad (34)$$

$\Gamma = 15 \mu\text{eV}$ has been chosen to approximate the measured dephasing time.²⁶ These operators represent all the possible spontaneous-emission pathways in the four-level system.

There are many equivalent ways to solve the master equation in terms of a nonlinear stochastic differential equation for a normalized state vector $|\psi\rangle$. We choose to use the quantum state diffusion equation³⁵

$$|d\psi\rangle = -\frac{i}{\hbar}H|\psi\rangle dt + \sum_j (\langle L_j^\dagger \rangle L_j - \frac{1}{2}L_j^\dagger L_j - \frac{1}{2}\langle L_j^\dagger \rangle \langle L_j \rangle) |\psi\rangle dt + \sum_j (L_j - \langle L_j \rangle) |\psi\rangle d\eta_j, \quad (35)$$

where $\langle L \rangle = \langle \psi | L | \psi \rangle$ and η_j are independent complex random variables. The density matrix can be expressed as $\rho = M|\psi\rangle\langle\psi|$, where M denotes ensemble average and the expectation value of any operator O is given by $M\langle\psi|O|\psi\rangle$. Inclusion of dephasing in this way reduces the fidelity for the shaped pulse sequence of MQFT from 0.992 to 0.892.

V. CONCLUSIONS

In the quantum control of multiexciton states in semiconductor quantum dots, we have shown that the use of composite pulses makes possible the realization of quantum operations in time scales of the order of a hundred femtoseconds. In addition to the theory of methods of constructing the pulses, we gave explicit examples to help experimental implementation. We adopted the concept of fidelity as a measure of the quality of a pulse sequence. We showed how to construct a sequence of pulses-based only on the physical σ_x and σ_y rotations. A numerical simulation of the application of the shaped pulses to the two-qubit quantum Fourier transform in a single semiconductor quantum dot provided a test of the pulse shaping. While the work so far provides a complete blueprint for an experimental demonstration of a simple quantum computation, future work for

a more realistic computer includes the interdot for scaling up the system, design of optical control to minimize decoherence, and design of optical implementation of quantum error corrections for digital control of decoherence and unintended dynamics.

ACKNOWLEDGMENTS

This work was supported by ARO F0005010, NSF DMR-0099572, and DARP ONR N0014-99-1-109. Y.S.D. acknowledges financial help from California Institute for Telecommunications & Information Technology.

APPENDIX

In this appendix the pulse sequences for the MQFT are constructed for an arbitrary number of qubits. From Eqs. (25) and (29), the action of MQFT and the inverse are given by

$$U_{\text{MQFT}}|x\rangle = \frac{1}{\sqrt{N}} \sum_{q=0}^{N-1} e^{2\pi i q \bar{x}/N} |q\rangle, \quad (A1)$$

$$U_{\text{MQFT}}^\dagger |q\rangle = \frac{1}{\sqrt{N}} \sum_{x=0}^{N-1} e^{-2\pi i q \bar{x}/N} |x\rangle. \quad (A2)$$

Define R_y to be a y rotation on all the qubits. Then,

$$\begin{aligned} R_y|x\rangle &\equiv \prod_j R_j(-\pi/2, \hat{y})|x\rangle \\ &= \frac{1}{\sqrt{N}} \sum_{p=0}^{N-1} \exp\left[\sum_{j=1}^n \pi i p_j (1-x_j)\right] |p\rangle. \end{aligned} \quad (A3)$$

Now consider the combined transformation

$$R_y U_{\text{MQFT}}^\dagger |q\rangle = \sum_{x=0}^{N-1} R_y|x\rangle \langle x| U_{\text{MQFT}}^\dagger |q\rangle = \frac{1}{N} \sum_{p=0}^{N-1} \sum_{x=0}^{N-1} \exp\left\{\left[\sum_{j=1}^n \pi i p_j (1-x_j)\right] - 2\pi i q \bar{x}/N\right\} |p\rangle \quad (A4)$$

$$= \frac{1}{N} \sum_{p=0}^{N-1} \prod_{j=1}^n \sum_{x_j=0}^1 \exp[\pi i (1-x_j)(p_j - \tilde{q} 2^{j-n})] |p\rangle \quad (A5)$$

$$= \sum_{p=0}^{N-1} \prod_{j=1}^n e^{-\pi i q^{(j)}/2} [\cos(\pi q^{(j)}/2) \delta_{q_j, p_j} + i \sin(\pi q^{(j)}/2) \delta_{q_j, 1-p_j}] |p\rangle \quad (A6)$$

$$= \sum_{p=0}^{N-1} \prod_{k=2}^n e^{i\alpha_k q_k} \prod_{j=1}^n [\cos(\pi q^{(j)}/2) \delta_{q_j, p_j} + i \sin(\pi q^{(j)}/2) \delta_{q_j, 1-p_j}] |p\rangle \quad (A7)$$

$$= \sum_{p=0}^{N-1} e^{i\alpha/2} \prod_{k=2}^n (e^{i\alpha_k/2} \delta_{q_k, 1} + e^{-i\alpha_k/2} \delta_{q_k, 0}) \prod_{j=1}^n [\cos(\pi q^{(j)}/2) \delta_{q_j, p_j} + i \sin(\pi q^{(j)}/2) \delta_{q_j, 1-p_j}] |p\rangle, \quad (A8)$$

where we use the definition $q^{(j)} = \sum_{k=j+1}^n q_k 2^{j-k}$. The α_k is defined through the relation $\prod_{j=1}^n e^{-\pi i q^{(j)}} = \prod_{k=2}^n e^{i \alpha_k q_k}$ and $\alpha = \sum_{k=2}^n \alpha_k$. Note that α_k depends only on k and N .

The two products in Eq. (A8) may be related to the rotations

$$\prod_{j=2}^n R_j(\alpha_k, \hat{z}) |q\rangle = \prod_{j=2}^n (e^{i \alpha_k / 2} \delta_{q_{k,1}} + e^{-i \alpha_k / 2} \delta_{q_{k,0}}) |q\rangle, \quad (\text{A9})$$

$$\begin{aligned} R_j(-\pi q^{(j)}, \hat{x}) &= R_j\left(-\pi \sum_{k=j+1}^n q_k 2^{j-k}, \hat{x}\right) \\ &= \prod_{k=j+1}^n C_{i,j}^{\text{ROT}}(-\pi 2^{j-k}, \hat{x}). \end{aligned} \quad (\text{A10})$$

These relations lead via

$$R U_{\text{MQFT}}^\dagger = e^{i \alpha / 2} \prod_{j=1}^n \prod_{k=j+1}^n C_{i,j}^{\text{ROT}}(-\pi 2^{j-k}, \hat{x}) \prod_{k=2}^n R_k(\alpha_k, \hat{z}) \quad (\text{A11})$$

to the conclusion that

$$\begin{aligned} U_{\text{MQFT}} &= e^{-i \alpha / 2} \prod_{j=1}^n \prod_{k=j+1}^n C_{k,j}^{\text{ROT}}(\pi 2^{j-k}, \hat{x}) \\ &\quad \times \prod_{l=2}^n R_l(-\alpha_l, \hat{z}) \prod_{m=1}^n R_m(-\pi/2, \hat{y}). \end{aligned} \quad (\text{A12})$$

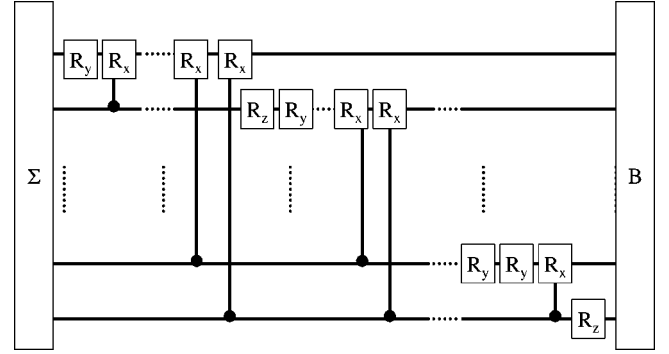


FIG. 5. Circuit diagram for QFT, Eq. (A12), with the operations in the order from left to right. Each horizontal line represents a qubit. The operations are explained in the text. The ones connecting two qubit lines represent logic gates of controlled rotations.

Note that $C_{k,j}^{\text{ROT}}$ may be moved to the right as in the circuit diagram of Fig. 5 but not past any rotation involving the target qubit j . Finally, by using $R(\alpha, z) = R(-\pi/2, y)R(\alpha, x)R(\pi/2, y)$ we obtain a pulse sequence, which involves only rotations and conditional rotations in the x , y direction to implement MQFT. Note that the total number of operations for n qubits is $O(n^2)$.

- ¹H. Rabitz, R. de Vivie-Riedle, M. Motzkus, and K. Kompa, *Science* **288**, 824 (2000).
- ²A. Haché, Y. Kostoulas, R. Atanasov, J. L. P. Hughes, J. E. Sipe, and H. M. van Driel, *Phys. Rev. Lett.* **78**, 306 (1997).
- ³A. P. Heberle, J. J. Baumberg, and K. Köhler, *Phys. Rev. Lett.* **75**, 2598 (1995).
- ⁴N. H. Bonadeo, J. Erland, D. Gammon, D. Park, D. S. Katzer, and D. G. Steel, *Science* **282**, 1473 (1998).
- ⁵D. D. Awschalom and J. M. Kikkawa, *Phys. Today* **52**(6), 33 (1999).
- ⁶B. E. Cole, J. B. Williams, B. T. King, M. S. Sherwin, and C. R. Stanley, *Nature (London)* **410**, 60 (2001).
- ⁷L. J. Sham and T. M. Rice, *Phys. Rev.* **144**, 708 (1966).
- ⁸M. Bayer, O. Stern, P. Hawrylak, S. Fafard, and A. Forchel, *Nature (London)* **405**, 923 (2000).
- ⁹A. Barenco, D. Deutsch, A. Ekert, and R. Jozsa, *Phys. Rev. Lett.* **74**, 4083 (1995).
- ¹⁰D. Loss and D. P. Di Vincenzo, *Phys. Rev. A* **57**, 120 (1998).
- ¹¹D. G. Sanders, K. W. Kim, and W. C. Holton, *Phys. Rev. B* **61**, 7526 (2000).
- ¹²T. A. Brun and H. Wang, *Phys. Rev. A* **61**, 032307 (2000).
- ¹³A. Imamoglu, D. D. Awschalom, G. Burkard, D. P. Di Vincenzo, D. Loss, M. Sherwin, and A. Small, *Phys. Rev. Lett.* **83**, 4204 (1999).
- ¹⁴M. S. Sherwin, A. Imamoglu, and T. Montroy, *Phys. Rev. A* **60**, 3508 (1999).
- ¹⁵F. Troiani, U. Hohenester, and E. Molinari, *Phys. Rev. B* **62**, R2263 (2000).
- ¹⁶P. Chen, C. Piermarocchi, and L. J. Sham, *Phys. Rev. Lett.* **87**, 067401 (2001).
- ¹⁷E. Biolatti, R. C. Iotti, P. Zanardi, and F. Rossi, *Phys. Rev. Lett.* **85**, 5647 (2000).
- ¹⁸L. Quiroga and N. F. Johnson, *Phys. Rev. Lett.* **83**, 2270 (1999).
- ¹⁹L. Viola, E. Knill, and S. Lloyd, *Phys. Rev. Lett.* **82**, 2417 (1999).
- ²⁰R. K. Shelton, L. S. Ma, H. C. Kapteyn, M. M. Murnane, J. L. Hall, and J. Ye, *Science* **293**, 1286 (2001).
- ²¹L. Allen and J. H. Eberly, *Optical Resonance and Two-Level Atoms* (Dover, New York, 1987), Chap. 1.
- ²²R. R. Ernst, G. Bodenhausen, and A. Wokaun, *Principles on Nuclear Magnetic Resonance in One and Two Dimensions* (Clarendon Press, Oxford, 1987), p. 72 *et seq.*
- ²³M. A. Nielsen and I. Chuang, *Quantum Computation and Quantum Information* (Cambridge University Press, Cambridge, 2000).
- ²⁴J. F. Poyatos, J. I. Cirac, and P. Zoller, *Phys. Rev. Lett.* **78**, 390 (1997).
- ²⁵A. Barenco and M. A. Dupertuis, *Phys. Rev. B* **52**, 2766 (1995).
- ²⁶N. H. Bonadeo, G. Chen, D. Gammon, D. S. Katzer, D. Park, and D. G. Steel, *Phys. Rev. Lett.* **81**, 2759 (1998).
- ²⁷T. Stievater, X. Li, D. G. Steel, D. Gammon, D. S. Katzer, D. Park, C. Piermarocchi, and L. J. Sham, *Phys. Rev. Lett.* **87**, 133603 (2001).
- ²⁸L. C. Andreani, G. Panzarini, and J.-M. Gérard, *Phys. Rev. B* **60**, 13 276 (1999).
- ²⁹R. M. Wilcox, *J. Math. Phys.* **8**, 962 (1967).
- ³⁰W. H. Press, S. A. Teukolsky, W. T. Vetterling, and B. P. Flannery,

Numerical Recipes (Cambridge University Press, Cambridge, 1986).

³¹G. P. Berman, D. K. Campbell and V. I. Tsifrinovich, *Phys. Rev. B* **55**, 5929 (1997).

³²Y. S. Weinstein, M. A. Pravia, E. M. Fortunato, S. Lloyd, and D. G. Cory, *Phys. Rev. Lett.* **86**, 1889 (2001).

³³Boustrophedon is writing that proceeds in one direction in one line (such as from left to right) and then in the reverse direction in the next line (such as from right to left). The term derives

from the way one would plow land with an ox, turning the ox back in the other direction at the end of a row. Boustrophedon is a more efficient way to both write and read, especially if your lines are very long. Some types of printers and their software print in this fashion.

³⁴H. Carmichael, *An Open Systems Approach to Quantum Optics* (Springer, Berlin, 1993).

³⁵N. Gisin and I. C. Percival, *J. Phys. A* **25**, 5677 (1992); R. Schack and T. A. Brun, *Comput. Phys. Commun.* **102**, 210 (1997).